ChemPubSoc Europe

DOI: 10.1002/cssc.201701526

CHEMSUSCHEM Full Papers

Diphenyl-2-pyridylamine-Substituted Porphyrins as Hole-Transporting Materials for Perovskite Solar Cells

Un-Hak Lee[+],[a, b] Randi Azmi[+],[c] Septy Sinaga,[c] Sunbin Hwang,[d] Seung Hun Eom,[a] Tae-Wook Kim,[d] Sung Cheol Yoon,*[a, b] Sung-Yeon Jang,*[c] and In Hwan Jung*[c]

The susceptibility of porphyrin derivatives to light-harvesting and charge-transport operations have enabled these materials to be employed in solar cell applications. The potential of porphyrin derivatives as hole-transporting materials (HTMs) for perovskite solar cells (PSCs) has recently been demonstrated, but knowledge of the relationships between the porphyrin structure and device performance remains insufficient. In this work, a series of novel zinc porphyrin (PZn) derivatives has been developed and employed as HTMs for low-temperature processed PSCs. Key to the design strategy is the incorporation of an electron-deficient pyridine moiety to down-shift the HOMO levels of porphyrin HTMs. The porphyrin HTMs incorporating diphenyl-2-pyridylamine (DPPA) have HOMO levels that are in good agreement with the perovskite active layers, thus facilitating hole transfers from the perovskite to the HTMs. The DPPA-containing zinc porphyrin-based PSCs gave the best performance, with efficiency levels comparable to those of PSCs using spiro-OMeTAD, a current state-of-the-art HTM. In particular, PZn–DPPA-based PSCs show superior air stability, in both doped and undoped forms, to spiro-OMeTAD based devices.

Introduction

Metal-coordinated porphyrin derivatives are essential chemicals in many fundamental biological functions, owing to their chemical stability, versatile redox activity, and intense absorption capabilities in the visible region. Hemes, which are iron-containing porphyrins, are responsible for oxygen transportation in the human body, and chlorophylls, magnesium-containing porphyrins, are essential pigments for light harvesting in plants.[1] Their ability with regard to light-to-charge conversion processes in biological system has inspired the development of artificial light-harvesting systems, such as dye-sensitized solar cells (DSSCs)[2] and organic photovoltaic devices (OPVs),[3] which demonstrate promising power conversion efficiencies (PCEs).

Although the light-harvesting and charge-transport properties of porphyrin derivatives have enabled their use as photoactive materials in solar cells,[2a–c, 3a–c, 4] their potential as hole-transporting materials (HTMs) for perovskite solar cells (PSCs) has also recently been proposed.[5] Yeh and co-workers developed porphyrin-based HTMs in which two ethynylaniline moieties are bonded to the porphyrin core horizontally and the other two alkoxyphenyl groups are bonded vertically.[6] Zhu and co-workers recently reported tetra-alkoxytriphenylamine-substituted porphyrin HTMs and studied the effects of metal ions in the central cavity of the porphyrin ring.[7] In these studies, a PCE of $>17\%$ was achieved by the fabrication of mesoporous PSC devices by using TiO_2 annealed at a high temperature as an electron-transporting material. Although the potential of porphyrin-based HTMs has been sufficiently demonstrated, the device PCEs have been somewhat lower than those of the current state-of-the-art HTM, 2,2′,7,7′-tetrakis(*N*,*N*-di-*p*-methoxyphenylamine)-9,9′-spirobifluorene (spiro-OMeTAD). Thus, the structural engineering of porphyrin HTMs in ways that can improve the energetic and electric properties is currently necessary for further development of these devices.

In this study, we have developed a series of novel zinc porphyrin (PZn) HTMs for PSCs and investigated the effects of the structural tuning of the device performance and charge extraction processes. The energy levels and intermolecular stacking of porphyrin HTMs were effectively manipulated by the incorporation of the diphenyl-2-pyridylamine (DPPA) moiety instead of triphenylamine (TPA). In our design strategy for porphyrin

[a] *U.-H. Lee,[+] Dr. S. H. Eom, Dr. S. C. Yoon*
Division of Advanced Materials
Korea Research Institute of Chemical Technology
Daejeon 34114 (Republic of Korea)
E-mail: yoonsch@krict.re.kr

[b] *U.-H. Lee,[+] Dr. S. C. Yoon*
Chemical Convergence Materials, University of Science and Technology
Daejeon 34113 (Republic of Korea)

[c] *R. Azmi,[+] S. Sinaga, Prof. S.-Y. Jang, Prof. I. H. Jung*
Department of Chemistry, Kookmin University
77 Jeongneung-ro, Seongbuk-gu, Seoul 02707 (Republic of Korea)
E-mail: syjang@kookmin.ac.kr
ihjung@kookmin.ac.kr

[d] *Dr. S. Hwang, Dr. T.-W. Kim*
Applied Quantum Composites Research Center
Institute of Advanced Composite Materials, Korea Institute of Science and Technology
Joellabuk-do 565-905 (Republic of Korea)

[+] *These authors contributed equally to this work.*

Supporting Information for this article is available under https://doi.org/10.1002/cssc.201701526.

This publication is part of dual Special Issues on "Perovskite Optoelectronics", published in *ChemSusChem* and *Energy Technology*. Please visit the *ChemSusChem* issue at **http://doi.org/10.1002/cssc.v10.19**, and the companion issue of *Energy Technology* at **http://dx.doi.org/10.1002/ente.v5.10**.

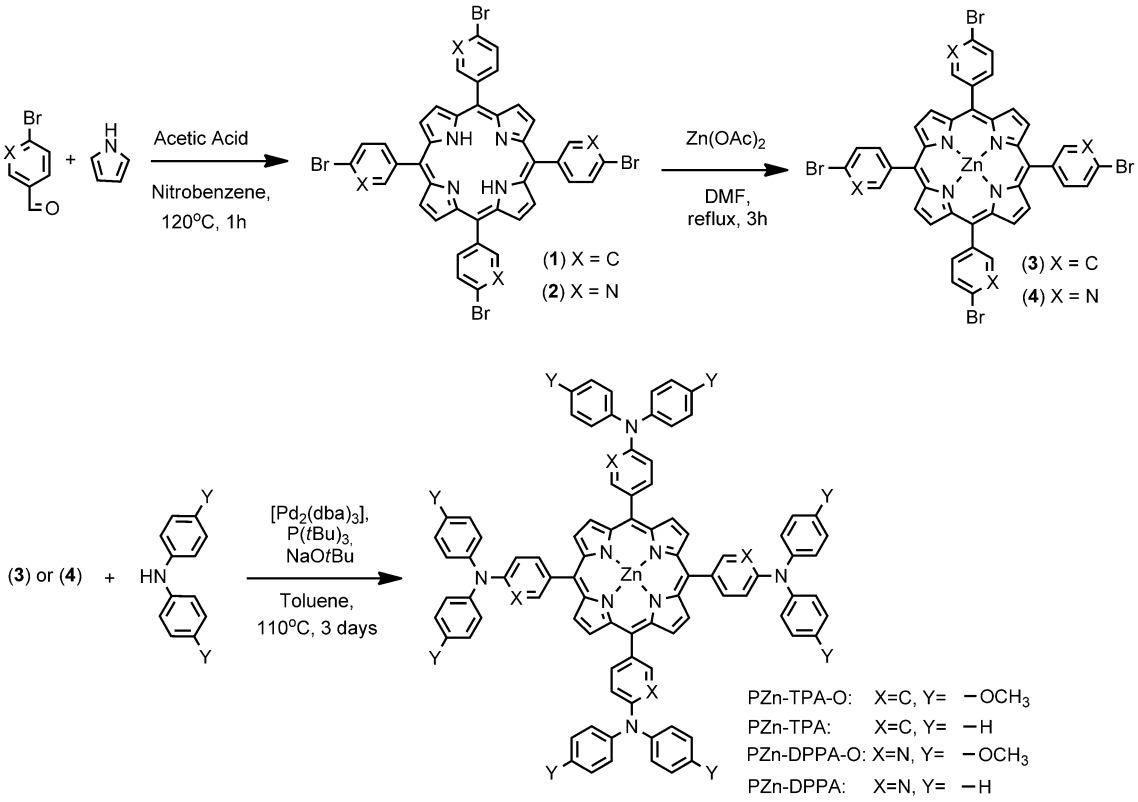

Scheme 1. Synthesis of porphyrin HTMs PZn–TPA-O, PZn–TPA, PZn–DPPA-O, and PZn–DPPA.

HTMs, electron-donating arylamine moieties are connected to the periphery of porphyrin cores to realize sufficient hole-transport properties (Scheme 1). To manipulate the energy levels by inductive effects, the pyridine moiety was incorporated as a linkage between the porphyrin core and arylamine substituents. Further tuning of the electron distribution through resonance effects was attempted by derivatizing methoxy groups on the arylamine substituents. The introduction of an electron-deficient pyridine ring into the proposed molecules achieved effective down-shifting of the HOMO energy level with enhanced charge transfer, whereas the addition of an electron-donating methoxy group raised the HOMO energy levels. Using the porphyrin HTMs, PSC devices processed at a low temperature were fabricated by using ZnO as an electron-transporting material (ETM) and methylammonium lead triiodide ($MAPbI_3$) perovskite by sequential deposition as an active layer. The PSC devices incorporating our DPPA-substituted zinc porphyrin HTM (PZn–DPPA) showed comparable PCEs to devices that used the current state-of-the-art HTM spiro-OMeTAD. In addition, PZn–DPPA was synthesized from relatively cheap starting materials, including pyrrole, diphenylamine, and 2-bromopyridine-5-carboxaldehyde, with only 3 steps, which is highly competitive in terms of synthetic cost compared to spiro-OMeTAD. This study of the relationship between the structural properties of our porphyrin molecules provides valuable information, which will benefit those seeking the further development of porphyrin-based HTMs.

Results and Discussion

The synthetic routes and structures of porphyrin HTMs used in this study are shown in Scheme 1, with details given in the Experimental section. 4-Bromobenzyl- or 4-bromopyridyl- substituted porphyrins were synthesized by a Diels–Alder reaction of pyrrole with 4-bromobenzaldehyde or 5-bromo-2-formylpyridine, respectively, resulting in corresponding yields of 43.7 and 29.7%.[8] All zinc porphyrin complexes were prepared by heating at refluxing in the presence of excess zinc acetate in DMF. Finally, 5,10,15,20-tetrakis{4-[*N*,*N*-di(4-methoxylphenyl)-aminophenyl]}porphyrin–zinc(II) (PZn–TPA-O), 5,10,15,20-tetrakis{4-[*N*,*N*-diphenylaminophenyl]}porphyrin–zinc(II) (PZn–TPA), 5,10,15,20-tetrakis{4-[*N*,*N*-di(4-methoxyphenyl)aminopyridinyl]}-porphyrin–zinc(II) (PZn–DPPA-O), and 5,10,15,20-tetrakis{4-[*N*,*N*-diphenylaminopyridinyl]}porphyrin–zinc(II) (PZn–DPPA) were synthesized by the Buchwald–Hartwig amination reaction of bromoporphyrins and diarylamines. The synthesized porphyrin HTMs showed good solubility in common organic solvents, such as chloroform, dichloromethane, and tetrahydrofuran, and were characterized by ^{1}H NMR spectroscopy and matrix-assisted laser desorption/ionization time-of-flight mass spectrometry (MALDI-TOF-MS).

The UV/Vis absorption spectra of porphyrin HTMs obtained in solution and film samples are shown in Figure 1. All porphyrin derivatives showed similar absorption patterns with one Soret and two Q bands in the 400–500 nm and 550–700 nm re-

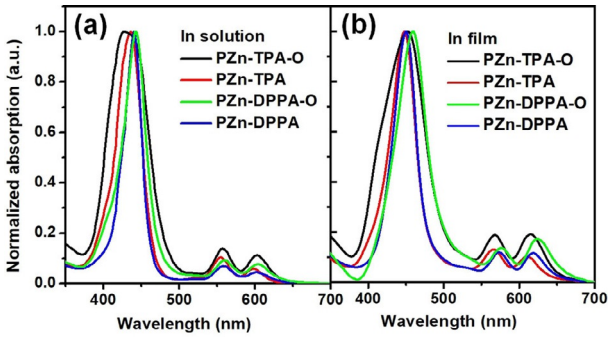

Figure 1. Absorption spectra of porphyrin derivatives: a) Solution in chloroform; b) film.

gions, respectively. By replacing TPA with DPPA, the absorptions were redshifted both in solution and film, indicating that the electron-accepting pyridine induces stronger intramolecular charge transfer (ICT) with the electron-donating porphyrin ring. As noted from the Soret band absorption characteristics, methoxy-substituted porphyrins (PZn–TPA-O and PZn–DPPA-O) have a broader range of absorption, both in the film and in solution, than unsubstituted porphyrins (PZn–TPA and PZn–DPPA) because the electron-donating methoxy groups generate more electronic transition states. The energy levels of the porphyrin HTMs were measured by ultraviolet photoelectron spectroscopy (UPS) and cyclic voltammetry (CV).[8] Particularly, the HOMO energy level significantly influences the hole-transfer properties from the perovskite active layers to the HTMs. The HOMO levels from the UPS spectra, determined by the valence band onset and secondary electron cut-off (E^{UPS}_{HOMO}; Figure 2a,b), were −5.13, −5.20, −5.23, and −5.36 eV for PZn–TPA-O, PZn–TPA, PZn–DPPA-O, and PZn–DPPA, respectively. The HOMO energy levels from the oxidation onset potential according to a CV analysis (E^{CV}_{HOMO}, Figure 2c) were in good agreement with the values from the UPS analysis. The optical characterization and energy level determination results are summarized in Table 1.

The energy level diagram of porphyrin HTMs constructed by using E^{UPS}_{HOMO} and the optical band gaps from the UV/Vis spectra are is depicted in Figure 2d. Incorporation of DPPA instead of TPA effectively down-shifted the HOMO energy levels of the HTMs by approximately 0.10–0.16 eV due to the decreased electron-donating effect from the arylamine moieties to the porphyrin core. On the other hand, the addition of *p*-methoxy units to arylamine moieties intensified the electron-donating effects by up-shifting the HOMO energy levels. The HOMO energy levels of porphyrin-based HTMs were readily controllable by manipulating either/both the pyridine incorporation characteristics or/and the *p*-methoxy group. Deeper HOMO levels of HTMs are advantageous for enhancing the open-circuit voltages (V_{OC}) of PSCs whereas matching with the perovskite HOMO level (−5.40 eV in this study) is beneficial for hole extraction.[9] The DPPA-incorporated PZn–DPPA had a HOMO level of −5.36 eV, which is suitable for effective hole extraction and V_{OC} enhancements in PSC devices. The lowest unoccupied molecular orbital (LUMO) levels of all porphyrin HTMs (−3.23 to −3.26 eV; Table 1) were sufficiently high compared to those of the perovskite layers (−3.90 eV), confirming the efficient blocking of unwanted electron transfer from $MAPbI_3$ to HTMs.[10]

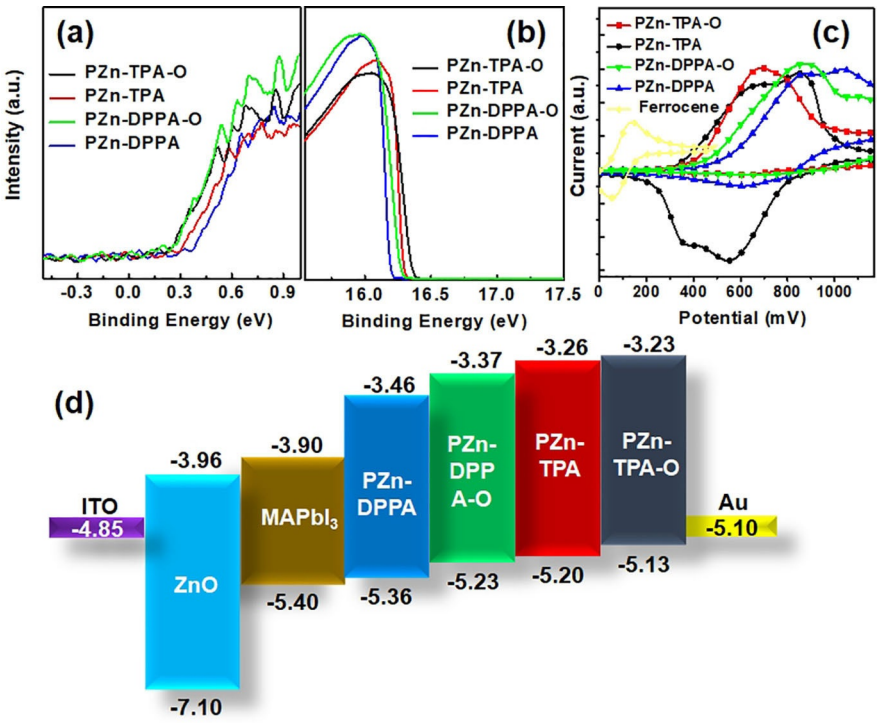

Figure 2. a,b) UPS spectra of the valence band region (a) and secondary electron cut-off region (b); c) cyclic voltammograms; d) energy-level diagram of the photovoltaic devices.

Table 1. Optical and electrochemical characterization results of porphyrin HTMs.

Type	λ_{max}		E_g^{opt}	Cyclic voltammetry			UPS	
	Solution[a]	Film[b]	[eV][c]	E_{ox} [V]	E_{HOMO}^{CV} [eV][d]	E_{cutoff} [eV]	E_i [eV]	E_{HOMO}^{UPS} [eV][e]
PZn–TPA-O	428, 558, 603	452, 568, 615	1.90	0.314	−5.08	16.36	−0.27	−5.13
PZn–TPA	436, 554, 598	448, 566, 610	1.94	0.382	−5.15	16.32	−0.30	−5.20
PZn–DPPA-O	442, 560, 604	460, 576, 624	1.86	0.435	−5.20	16.27	−0.28	−5.23
PZn–DPPA	440, 558, 602	450, 573, 618	1.90	0.539	−5.30	16.22	−0.36	−5.36

[a] In dilute chloroform. [b] On quartz plates. [c] Band gap calculated from the absorption onset wavelength in film. [d] HOMO levels determined from the onset of the first oxidation potential (E_{ox}). [e] HOMO levels determined from the E_{cutoff} and E_i values from the UPS analysis.

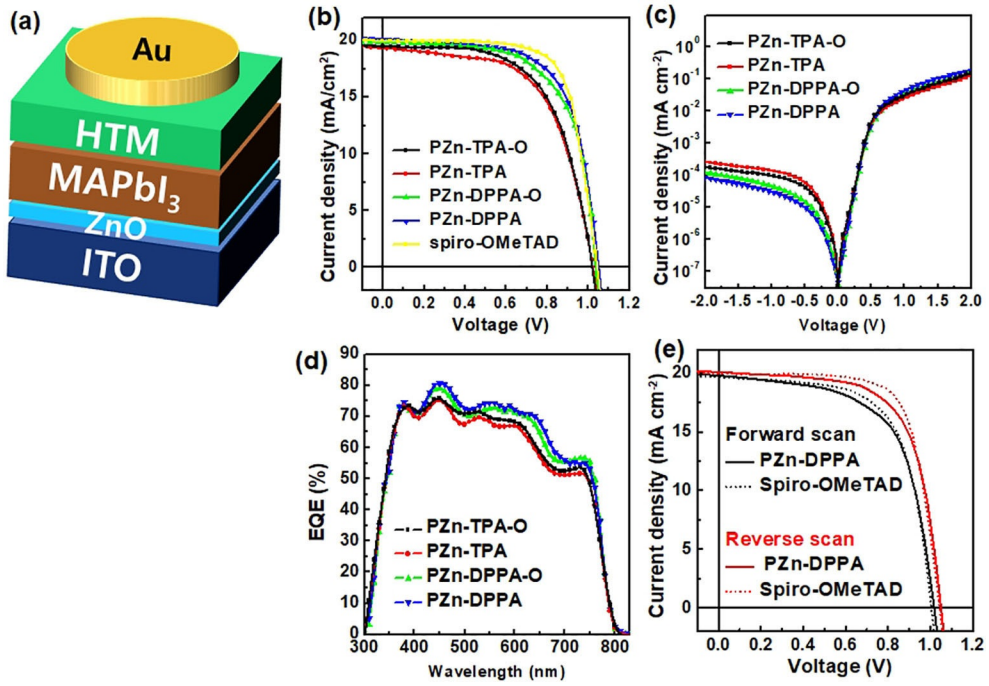

Figure 3. a) The architecture of a low-temperature-processed PSC; b) *J–V* characteristics of PSCs by reverse scan under AM 1.5G one sun illumination (100 mW cm^{-2}); c) *J–V* characteristics in the dark; d) external quantum efficiency (EQE) spectra of PSCs; e) *J–V* curves of PZn–DPPA- and spiro-OMeTAD-based PSCs by forward or reverse scan.

Low-temperature planar PSCs were fabricated with the configuration ITO/ZnO/$MAPbI_3$/HTM/Au (Figure 3a; ITO = indium-doped tin oxide). ZnO layers created by in situ sol–gel conversion (annealing at 140 °C) were used as ETMs and sequentially deposited $MAPbI_3$ (annealing at 100 °C) was used as the perovskite active layer. The porphyrin HTMs were spin-coated onto the perovskite layers at room temperature. The detailed procedures of the device fabrication process are given in the Experimental section. The current density–voltage (*J–V*) characteristics under AM 1.5G illumination (100 mW cm^{-2}) by reverse scan are shown in Figure 3b and the results are summarized in Table 2. The PZn–DPPA-based devices showed the highest PCE of 14.11%, whereas the devices using PZn–TPA-O, PZn–TPA, and PZn–DPPA-O showed lower PCEs of 12.40, 11.96, and 13.52%, respectively. The PCE of the PZn–DPPA device is comparable to that of spiro-OMeTAD-based devices (14.61%; Figure 3b and Table 2). The short-circuit current density (J_{SC}) values according to *J–V* measurements were in good agreement with the calculated J_{SC} values from an external quantum efficiency (EQE) analysis (Figure 3d) with a mismatch of <4%. The statistics of the device PCEs are shown in Figure S5 (see the Supporting Information). The *J–V* curves of PZn–DPPA device by forward and reverse scan (Figure 3e) showed a similar hysteresis to the spiro-OMeTAD device. The *J–V* curves of all devices studied are shown in Figure S6.

The V_{OC} values of PSCs are influenced by the HOMO levels of the HTMs; thus, the PZn–DPPA device showed the highest

Table 2. Summary of PSC performances.

Type	V_{OC} [V]	J_{SC} [mA cm^{-2}]	*FF*	R_S[a] [Ω cm^{-2}]	R_{SH}[b] [Ω cm^{-2}]	PCE [%]
PZn–TPA-O	1.031	19.76	0.61	23.56	645	12.40
PZn–TPA	1.036	19.35	0.60	24.38	612	11.96
PZn–DPPA-O	1.043	20.28	0.64	22.12	784	13.52
PZn–DPPA	1.054	20.74	0.65	20.04	823	14.11
spiro-OMeTAD	1.047	20.58	0.68	20.64	1078	14.61

[a] R_S: Series resistance. [b] R_{SH}: Shunt resistance.

value of 1.054 V, owing to its deepest HOMO level (−5.36 eV). The superior J_{SC} value of the PZn–DPPA device originated from the improved charge extraction throughout the visible range, as indicated by the external quantum efficiency (EQE) spectra (Figure 3 d). The highest rectification ratio of PZn–DPPA devices, shown in dark *J–V* characteristics (Figure 3 c), indicated their superior charge selectivity, thus enabling improved fill factors (*FF*s) in devices. The effects of the energetic and electric properties of the HTMs on device performance capabilities and the charge-collection efficiency are further elucidated below.

The hole-transfer characteristics at the $MAPbI_3$/HTM interfaces were investigated by using steady-state photoluminescence (PL) spectroscopy. Various perovskite/HTM junctions were formed on glass substrates and the PL intensity from the $MAPbI_3$ perovskite layers were measured (Figure 4 a). The PL of

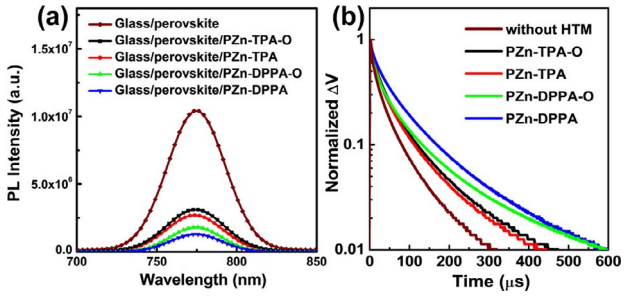

Figure 4. a) Steady-state PL spectra of various $MAPbI_3$/HTM samples; b) TPV decay curves.

the pristine $MAPbI_3$ layer was significantly reduced when the interfaces with the porphyrin HTMs were formed, confirming the hole transfer from $MAPbI_3$ to the HTMs.[11] The decrease of the PL intensity was strongly dependent on the HOMO levels of the porphyrin HTMs. As the HOMO energy level of the porphyrin HTM becomes closer to that of $MAPbI_3$, hole transfer is facilitated.[11a,b] The hole-transport properties within the porphyrin HTM layers were revealed by measuring the space-charge-limited-current (SCLC) values of hole-only devices (ITO/poly(3,4-ethylenedioxythiophene)-poly(styrenesulfonate) (PEDOT:PSS)/HTM/MoO_3/Ag). The current–voltage (*I–V*) responses of the hole-only devices are shown in Figure S**7**. The hole mobility values were calculated from linear fitting in the SCLC regime using Mott–Gurney model[12] (Table S1). PZn–DPPA gave rise to a hole mobility value of 4.10×10^{-4} $cm^2V^{-1}s^{-1}$, which is comparable to that of spiro-OMeTAD (4.22×10^{-4} $cm^2V^{-1}s^{-1}$). Two DPPA-containing HTMs (PZn–DPPA and PZn–DPPA-O) showed greater hole mobility than the TPA-based HTMs (PZn–TPA and PZn–TPA-O). This improved hole mobility in DPPA-incorporated porphyrin HTMs can be attributed to the enhanced molecular stacking, as indicated by two-dimensional grazing-incidence X-ray diffraction (2 D-GIXD). The PZn–DPPA film showed enhanced face-on π–π stacking compared to the PZn–TPA film (Figure S8). The (010) out-of-plane (Q_z) peaks at around 1.70 $Å^{-1}$ correspond to an intermolecular π–π distance of about 3.70 Å. This improved face-on orientation may have promoted vertical charge transport, resulting in greater SCLC hole mobility in the PZn–DPPA film.

Subsequently, we investigated the effects of porphyrin HTMs on the charge-extraction properties of PSCs. The charge-recombination lifetime (τ_{rec}) of PSCs was determined by means of transient photovoltage (TPV) spectroscopy. In this case, the transient voltage decay curves (Figure 4 b) are fitted to a mono-exponential decay function to obtain τ_{rec}. The PZn–DPPA device also showed a longer lifetime (78.11 μs) than the PZn–TPA device (69.12 μs), revealing superior charge extraction (Table S2).[13] The intensity-modulated photocurrent/photovoltage (IMPS/IMVS) method was also used to ascertain the charge-recombination/transport properties of the devices (Figure 5 a, b). The charge-transport time (τ_{ct}) and charge-recombination lifetime (τ_r) of each device were obtained from the frequency minimum in the Nyquist plot following $\tau_{ct,r}={}^1/_2\,\pi f_{min}$ (IMPS, IMVS).[14] Consistent with the TPV analysis results, PZn–DPPA devices showed the highest charge transport with reduced recombination times (lowest τ_{ct} value, 0.12 ms, and highest τ_r value, 0.35 ms) compared to other porphyrin-HTM-based devices (Table S3).

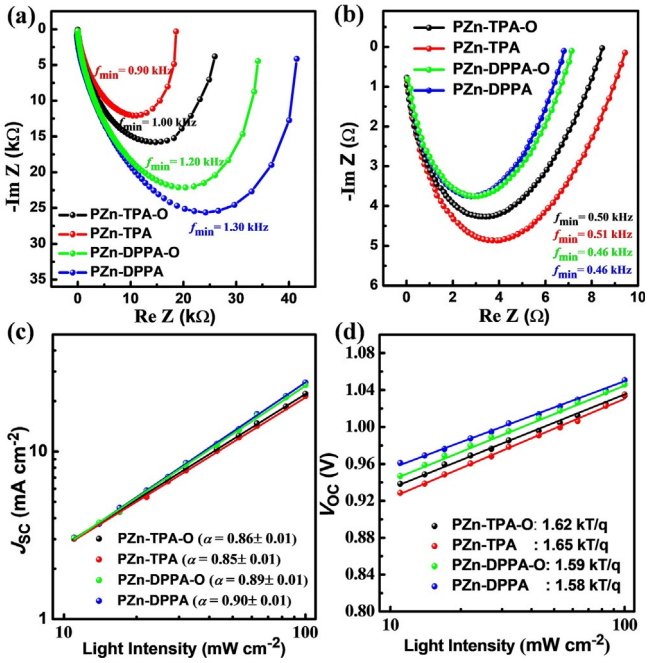

Figure 5. Analysis results of the charge-extraction properties: a) IMPS; b) IMVS; c) J_{SC} vs. illumination intensity; d) V_{OC} vs. illumination intensity.

To elucidate the recombination mechanisms of PSCs, the *J–V* characteristics were examined as a function of the illumination intensity. Figure 5 c shows the power law dependence of J_{SC} on the illumination intensity ($J_{SC}\propto I^{\alpha}$), where *I* is the light intensity and α is an exponential factor.[15] The α values of PSCs using DPPA-containing HTMs (PZn–DPPA and PZn–DPPA-O) were in the range of 0.89–0.90, whereas those using TPA-containing HTMs (PZn–TPA and PZn–TPA-O) showed much lower α values (0.85–0.86). The highest α value of 0.90 in a PZn–DPPA device revealed the fewest bimolecular recombinations under short-

circuit conditions. The slope of V_{OC} versus the illumination intensity (Figure 5d) indicates the probability of trap-assisted recombination under open-circuit conditions.[15a,16] The lowest slope of the PZn–DPPA devices ($1.58kTq^{-1}$) indicated the fewest trap-assisted recombinations among the devices studied here. The well-matched energy levels, high hole mobility, and reduced interfacial charge recombinations of PZn–DPPA effectively improved the charge-extraction properties of the PSCs, demonstrating performances comparable to those of spiro-OMeTAD-based devices.

The long-term stabilities of PZn–DPPA and spiro-OMeTAD devices in ambient air were evaluated (Figure 6). The devices were kept without encapsulation and the PCEs under AM 1.5G one sun illumination (100 mW cm^{-2}) were measured every few

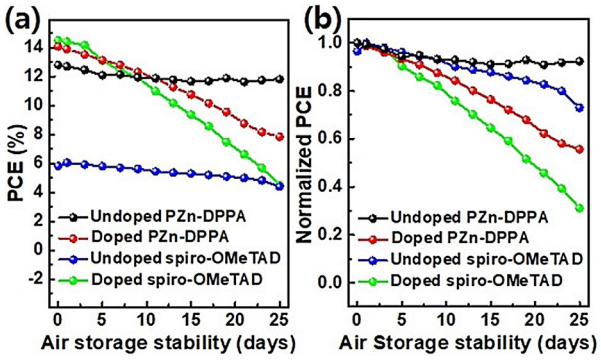

Figure 6. a) Long-term air stability of PSCs incorporating PZn–DPPA and spiro-OMeTAD with or without dopant; b) normalized PCEs of the corresponding devices.

days in an ambient air atmosphere. For each HTM, both with doped and undoped forms were employed to fabricate PSCs. The PZn–DPPA devices showed superior stability to spiro-OMeTAD devices regardless of doping. After 25 days, the doped PZn–DPPA device retained 56% of its initial PCE, whereas the doped spiro-OMeTAD device retained only 31%. When we used undoped PZn–DPPA, the device PCE was slightly lowered compared to the doped form. However, the air-stability was improved significantly (92% retention after 25 days). In contrast, the device using undoped spiro-OMeTAD showed substantially lower PCE (6.1%), whereas the air stability was improved (73% retension after 25 days). The hydrophobicity of PZn–DPPA contributed to enhanced air stability, while the face-on orientation offered relatively high hole transport in its undoped form. The sufficient hole-transporting property of PZn–DPPA without dopant will be beneficial for future design for dopant-free porphyrin-based HTMs.

Conclusions

We developed a series of novel porphyrin derivatives (PZn–TPA-O, PZn–TPA, PZn–DPPA-O, and PZn–DPPA) and employed them as hole-transporting materials (HTMs) for low-temperature perovskite solar cells (PSCs). The effects of their chemical structures on the PSCs' energetic and electric properties and device performance capabilities were studied. We revealed that the incorporation of DPPA into a porphyrin core is a useful strategy for the design of porphyrin-based HTMs. Connecting a DPPA moiety to a porphyrin core effectively down-shifted the HOMO levels in comparison to the TPA moiety, providing a better match to $MAPbI_3$ perovskite active layers. Incorporation of the DPPA moiety also improved the hole mobility of porphyrin HTMs by enhancing face-on molecular stacking. Given the energetic and electric benefits of DPPA incorporation, the charge-extraction properties of the PSCs were improved. The PZn–DPPA-based devices gave PCEs increased by 18% compared to PZn–TPA-based devices. The PCE of the PZn–DPPA-based PSC was comparable to those of PSCs incorporating spiro-OMeTAD, a current state-of-the-art HTM. Importantly, the PZn–DPPA-based devices showed much improved air stability in both doped and undoped forms compared to spiro-OMeTAD. This study of the relationship between the structure and properties of porphyrin-based HTMs provides valuable information for the further development of HTMs for PSCs.

Experimental Section

Synthesis of HTMs

5,10,15,20-Tetrakis(4-bromophenyl)porphyrin (**1**): 4-bromobenzaldehyde (3.72 g, 20.1 mmol) was dissolved in nitrobenzene (100 mL) and acetic acid (150 mL). The reaction mixture was heated to 120 °C, and then freshly distilled pyrrole (1.55 g, 23.1 mmol) was slowly added. The solution color changed from yellow to dark brown over 1 h. After reaction was completed, the mixture was cooled slowly to room temperature and methanol (100 mL) was poured into the mixture to prevent solvent freezing. The solution was stored in refrigerator at −20 °C. A few hours later, the cooled mixture was filtered under reduced pressure. The removed solid was rinsed with methanol (300 mL) and pure **1** was obtained as a purple solid without further purification (2.04 g, 43.7%). ^{1}H NMR ($CDCl_3$, 400 MHz): $\delta = 8.94$ (s, 8H), 8.06 (d, $J = 8.4$ Hz, 8H), 7.89 ppm (d, $J = 8.0$ Hz, 8H).

5,10,15,20-Tetrakis(5-bromopyridin-2-yl)porphyrin (**2**): Compound **2** was synthesized according to a similar synthetic procedure to compound **1**, by using 2-bromopyridine-5-carboxaldehyde (1.73 g, 9.3 mmol), nitrobenzene (50 mL), acetic acid (75 mL), and distilled pyrrole (0.72 g, 10.7 mmol) to give a purple solid (644 mg, 29.7%). ^{1}H NMR ($CDCl_3$, 400 MHz): $\delta = 9.19$ (s, 4H), 8.89 (s, 8H), 8.38 (dd, 4H), 7.98 ppm (d, $J = 8.0$ Hz, 4H).

5,10,15,20-Tetrakis(4-bromophenyl)porphyrin zinc(II) (**3**): Compound **1** (2.00 g, 2.15 mmol) and zinc acetate (1.78 g, 9.7 mmol) were dissolved in dry DMF (50 mL). The resulting mixture was stirred at 120 °C with reflux for 1 day. The resulting mixture was stored in a refrigerator at −20 °C. After a few hours, the cooled mixture was filtered under reduced pressure. The removed solid was rinsed with methanol (300 mL) to give **3** as a shiny purple solid (1.88 g, 86.2%), which was used without further purification for next step.

5,10,15,20-Tetrakis(5-bromopyridin-2-yl)porphyrin zinc(II) (**4**): Compound **2** (640 mg, 0.642 mmol) and zinc acetate (0.53 g, 2.90 mmol) were dissolved in dry DMF (25 mL). The reaction and purification were carried out according to a similar synthetic proce-

dure to compound **3** to give product **4** (572 mg, 83.5%), which was used without further purification for next step.

5,10,15,20-Tetrakis(4-diphenylaminophenyl)porphyrin zinc(II) (PZn–TPA): Tri-*tert*-butylphosphine (102 mg, 0.51 mmol) and $[Pd_2(dba)_3]$ (25 mg, 0.027 mmol) were dissolved in anhydrous toluene (15 mL). Compound **3** (250 mg, 0.25 mmol), sodium *tert*-butoxide (102 mg, 1.07 mmol), and diphenylamine (181 mg, 1.07 mmol) were successively added to the reaction mixture. The solution was heated at reflux for 4 days under a nitrogen atmosphere and then cooled down to room temperature. After extraction with dichloromethane (200 mL) and water (75 mL), the organic layer was collected and the solvent removed by evaporation under reduced pressure. The solid residue was purified by column chromatography on silica gel with 3:1 CH_2Cl_2/*n*-hexanes as the eluent to obtain the product as a dark purple solid (220 mg, 65.4%). ^{1}H NMR ($CDCl_3$, 400 MHz): $\delta =$ 9.09 (s, 8H), 8.07 (d, $J = 6.8$ Hz, 8H), 7.41–7.47 (m, 40H), 7.13 ppm (d, $J = 8.0$ Hz, 8H); MALDI-TOF-MS: *m/z* calcd for $C_{92}H_{64}N_8Zn$: 1346.9 $[M]^+$; found 1362.5

4,4′,4″-(20-{4-[(3-Methoxyphenyl)(4-methoxyphenyl)amino]phenyl}-porphyrin-5,10,15-triyl)tris[*N*,*N*-bis(4-methoxyphenyl)aniline] zinc(II) (PZn–TPA-O): PZn–TPA-O was synthesized according to a similar synthetic procedure to PZn–TPA. *o*-Methoxydiphenylamine (245 mg, 1.07 mmol) was used instead of diphenylamine. The final product was obtained by column chromatography on silica gel with 1:2 CH_2Cl_2/*n*-hexanes as the eluent (307 mg, 77.2%). ^{1}H NMR ($CDCl_3$, 400 MHz): $\delta = 9.08$ (s, 8H), 7.99 (d, $J = 8.0$ Hz, 8H), 7.38–7.29 (m, 32H), 6.96 (d, $J = 8.0$ Hz, 8H), 3.86 ppm (s,12H); MALDI-TOF-MS: *m/z* calcd for $C_{100}H_{80}N_8O_8Zn$: 1587.1 $[M]^+$; found 1586.4.

5,5′,5″,5‴-(Porphyrin-5,10,15,20-tetrayl)tetrakis(*N*,*N*-diphenylpyridyl-2-amine) zinc(II) (PZn–DPPA): PZn–DPPA was synthesized according to a similar synthetic procedure to PZn–TPA. Compound **4** (250 mg, 0.25 mmol) was used instead of compound **3**. The dark green final product was purified by column chromatography on silica gel with 3:1 CH_2Cl_2/*n*-hexanes as the eluent (173 mg, 51.2%). ^{1}H NMR ($CDCl_3$, 400 MHz): $\delta = 9.11$ (s, 8H), 8.99 (s, 4H), 8.28 (d, 4H), 7.48 (m, 40H), 7.16 ppm (d, $J = 6.4$ Hz, 4H); MALDI-TOF-MS: *m/z* calcd for $C_{88}H_{60}N_{12}Zn$: 1350.9 $[M]^+$; found 1365.3.

5,5′,5″-(20-{6-[(3-Methoxyphenyl)(4-methoxyphenyl)amino]pyridin-3-yl}porphyrin-5,10,15-triyl)tris[*N*,*N*-bis(4-methoxyphenyl)pyridyl-2-amine] zinc(II) (PZn–DPPA-O): PZn–DPPA-O was synthesized according to a similar synthetic procedure to PZn–TPA. Compound **4** (250 mg, 0.25 mmol) and *o*-methoxydiphenylamine (253 mg, 1.10 mmol) were used instead of compound **3** and diphenylamine. The dark green final product was purified by column chromatography on silica gel with 1:2 CH_2Cl_2/*n*-hexanes as the eluent (273 mg, 68.5%). ^{1}H NMR ($CDCl_3$, 400 MHz): $\delta = 9.10$ (s, 8H), 8.96 (s, 4H), 8.21 (d, 4H), 7.47 (br, 16H), 7.01 ppm (br, 20H); MALDI-TOF-MS: *m/z* calcd for $C_{96}H_{76}N_{12}O_8Zn$: 1591.1 $[M]^+$; found 1589.4.

Device fabrication

The ITO substrate was washed in acetone and isopropyl alcohol before use followed by UV ozone treatment. ZnO electron accepting layer (EAL) were fabricated by in situ sol–gel conversion according to a previously reported method.[14c,17] The ZnO sol–gel solution was spin-coated on ITO/glass substrates at 2000 rpm for 15 s then annealed at 140 °C for 10 min for a thickness of approximately 40 nm. The $MAPbI_3$ layers were deposited by a sequential deposition method, according to a slightly modified reported procedure.[18] A mixture of PbI_2 (1 mol) and DMSO (1 mol) in DMF (1 mL) was heated at 100 °C for 10 h. Firstly, the PbI_2 solution was spin-coated (3000 rpm for 20 s) on ITO/ZnO substrate followed by thermal annealing at 100 °C for 3 min. After cooling for several minutes, the PbI_2 layers were dipped into a 0.25 mM methylammonium iodide (MAI) solution in 2-propanol for 1 min. The film was then immersed into 2-propanol to removed removing excess MAI. Finally, the films were annealed at 100 °C for 5 min to yield $MAPbI_3$ perovskite layers. The hole-transporting layer solution was spin-coated at 4000 rpm for 30 sec. The solution of each PZn-based HTM contained 35 mM HTM in chlorobenzene (1 mL) with 16 mM LiTFSI and 96 mM TBP additives. The solution of spiro-OMeTAD, contained 61 mM spiro-OMeTAD in chlorobenzene 1 mL) with 31 mM LiTFSI and 191 mM TBP additives. All fabrication processes were done under ambient air conditions. For the metal electrode, 80 nm thick Au was deposited by using thermal evaporation at low pressure ($< 10^{-6}$ torr) with metal mask (area = 7.07 mm^2).

Device analysis

J–V profiles were recorded by using a Keithley 2401 source unit with a 150 W Xenon lamp under AM 1.5 G (100 mW cm^{-2}) illumination (Newport). The spectral mismatch was calibrated by using a KG-5 filter covered by monosilicon detector. The external quantum efficiency (EQE) spectra were obtained by passing the output of a 400 W Xenon lamp through a monochromator and using the appropriate order-sorting filters. The collimated output of the monochromator was measured through a 1 mm aperture with calibrated Newport 818-UV and 818-IR power meters. The wavelength values were scanned at a chopping frequency of 5 Hz from 300 nm to 830 nm.

Acknowledgements

The authors gratefully acknowledge support from the New and Renewable Energy Core Technology Program of the Korea Institute of Energy Technology Evaluation and Planning (KETEP), granted financial resources from the Ministry of Trade, Industry and Energy, Republic of Korea (No. 20163030013960), the Technology Innovation Program (No.10077471) funded By MOTIE, Korea, the Technology Development Program to Solve Climate Changes of the National Research Foundation (NRF) funded by the Ministry of Science, ICT & Future Planning (NRF-2016M1A2A2940912), the National Research Foundation (NRF) grant funded by the Korean Government (MSIP, No. 2016R1A5A1012966, No. 2017R1A2B2009178, No. 2017M2A2A6A01020854 and No. 2017R1C1B2010694), and the Global Scholarship Program for Foreign Graduate Students at Kookmin University in Korea.

Conflict of interest

The authors declare no conflict of interest.

Keywords: diphenyl-2-pyridylamine · hole transporting materials · low-temperature process · perovskite solar cells · porphyrin

[1] a) J. A. Shelnutt, X.-Z. Song, J.-G. Ma, S.-L. Jia, W. Jentzen, C. J. Medforth, C. J. Medforth, *Chem. Soc. Rev.* **1998**, *27*, 31–42; b) W. T. Hadmojo, D. Yim, H. Aqoma, D. Y. Ryu, T. J. Shin, H. W. Kim, E. Hwang, W.-D. Jang,

I. H. Jung, S.-Y. Jang, *Chem. Sci.* **2017**, *8*, 5095 – 5100; c) W. Kühlbrandt, D. N. Wang, *Nature* **1991**, *350*, 130 – 134.

[2] a) J. Kesters, P. Verstappen, M. Kelchtermans, L. Lutsen, D. Vanderzande, W. Maes, *Adv. Energy Mater.* **2015**, *5*, 1500218; b) M. Urbani, M. Grätzel, M. K. Nazeeruddin, T. Torres, *Chem. Rev.* **2014**, *114*, 12330 – 12396; c) A. Yella, C.-L. Mai, S. M. Zakeeruddin, S.-N. Chang, C.-H. Hsieh, C.-Y. Yeh, M. Grätzel, *Angew. Chem. Int. Ed.* **2014**, *53*, 2973 – 2977; *Angew. Chem.* **2014**, *126*, 3017 – 3021; d) S. Mathew, A. Yella, P. Gao, R. Humphry-Baker, F. E. CurchodBasile, N. Ashari-Astani, I. Tavernelli, U. Rothlisberger, K. NazeeruddinMd, M. Grätzel, *Nat. Chem.* **2014**, *6*, 242 – 247; e) M. Ishida, D. Hwang, Z. Zhang, Y. J. Choi, J. Oh, V. M. Lynch, D. Y. Kim, J. L. Sessler, D. Kim, *ChemSusChem* **2015**, *8*, 2967 – 2977; f) R. G. W. Jinadasa, B. Li, B. Schmitz, S. Kumar, Y. Hu, L. Kerr, H. Wang, *ChemSusChem* **2016**, *9*, 2239 – 2249.

[3] a) T. Higashino, H. Imahori, *Dalton Trans.* **2015**, *44*, 448 – 463; b) K. Gao, L. Li, T. Lai, L. Xiao, Y. Huang, F. Huang, J. Peng, Y. Cao, F. Liu, T. P. Russell, R. A. J. Janssen, X. Peng, *J. Am. Chem. Soc.* **2015**, *137*, 7282 – 7285; c) L. Nian, K. Gao, F. Liu, Y. Kan, X. Jiang, L. Liu, Z. Xie, X. Peng, T. P. Russell, Y. Ma, *Adv. Mater.* **2016**, *28*, 8184 – 8190; d) K. Zhang, K. Gao, R. Xia, Z. Wu, C. Sun, J. Cao, L. Qian, W. Li, S. Liu, F. Huang, X. Peng, L. Ding, H.-L. Yip, Y. Cao, *Adv. Mater.* **2016**, *28*, 4817 – 4823.

[4] A. Zhang, C. Li, F. Yang, J. Zhang, Z. Wang, Z. Wei, W. Li, *Angew. Chem. Int. Ed.* **2017**, *56*, 2694 – 2698; *Angew. Chem.* **2017**, *129*, 2738 – 2742.

[5] H. Imahori, T. Umeyama, K. Kurotobi, Y. Takano, *Chem. Commun.* **2012**, *48*, 4032 – 4045.

[6] H.-H. Chou, Y.-H. Chiang, M.-H. Li, P.-S. Shen, H.-J. Wei, C.-L. Mai, P. Chen, C.-Y. Yeh, *ACS Energy Lett.* **2016**, *1*, 956 – 962.

[7] S. Chen, P. Liu, Y. Hua, Y. Li, L. Kloo, X. Wang, B. Ong, W.-K. Wong, X. Zhu, *ACS Appl. Mater. Interfaces* **2017**, *9*, 13231 – 13239.

[8] I. H. Jung, J.-H. Kim, S. Y. Nam, C. Lee, D.-H. Hwang, S. C. Yoon, *Macromolecules* **2015**, *48*, 5213 – 5221.

[9] S. Ryu, J. H. Noh, N. J. Jeon, Y. C. Kim, W. S. Yang, J. Seo, S. I. Seok, *Energy Environ. Sci.* **2014**, *7*, 2614 – 2618.

[10] a) Y. Song, S. Lv, X. Liu, X. Li, S. Wang, H. Wei, D. Li, Y. Xiao, Q. Meng, *Chem. Commun.* **2014**, *50*, 15239 – 15242; b) J. Zhang, Y. Hua, B. Xu, L. Yang, P. Liu, M. B. Johansson, N. Vlachopoulos, L. Kloo, G. Boschloo, E. M. J. Johansson, L. Sun, A. Hagfeldt, *Adv. Energy Mater.* **2016**, *6*, 1601062.

[11] a) J. H. Kim, P.-W. Liang, S. T. Williams, N. Cho, C.-C. Chueh, M. S. Glaz, D. S. Ginger, A. K.-Y. Jen, *Adv. Mater.* **2015**, *27*, 695 – 701; b) P. Docampo, J. M. Ball, M. Darwich, G. E. Eperon, H. J. Snaith, *Nat. Commun.* **2013**, *4*, 2761; c) J. H. Heo, S. H. Im, J. H. Noh, T. N. Mandal, C.-S. Lim, J. A. Chang, Y. H. Lee, H.-j. Kim, A. Sarkar, M. K. Nazeeruddin, M. Grätzel, S. I. Seok, *Nat. Photonics* **2013**, *7*, 486 – 491; d) Y. S. Kwon, J. Lim, H.-J. Yun, Y.-H. Kim, T. Park, *Energy Environ. Sci.* **2014**, *7*, 1454 – 1460.

[12] V. D. Mihailetchi, J. Wildeman, P. W. M. Blom, *Phys. Rev. Lett.* **2005**, *94*, 126602.

[13] D. Bi, L. Yang, G. Boschloo, A. Hagfeldt, E. M. J. Johansson, *J. Phys. Chem. Lett.* **2013**, *4*, 1532 – 1536.

[14] a) A. Pockett, G. E. Eperon, T. Peltola, H. J. Snaith, A. Walker, L. M. Peter, P. J. Cameron, *J. Phys. Chem. C* **2015**, *119*, 3456 – 3465; b) Y. Zhao, K. Zhu, *J. Phys. Chem. Lett.* **2013**, *4*, 2880 – 2884; c) R. Azmi, S. Sinaga, H. Aqoma, G. Seo, T. K. Ahn, M. Park, S.-Y. Ju, J.-W. Lee, T.-W. Kim, S.-H. Oh, S.-Y. Jang, *Nano Energy* **2017**, *39*, 86 – 94.

[15] a) R. Azmi, S.-H. Oh, S.-Y. Jang, *ACS Energy Lett.* **2016**, *1*, 100 – 106; b) V. D. Mihailetchi, H. X. Xie, B. de Boer, L. J. A. Koster, P. W. M. Blom, *Adv. Funct. Mater.* **2006**, *16*, 699 – 708.

[16] M. M. Mandoc, W. Veurman, L. J. A. Koster, B. de Boer, P. W. M. Blom, *Adv. Funct. Mater.* **2007**, *17*, 2167 – 2173.

[17] a) R. Azmi, H. Aqoma, W. T. Hadmojo, J.-M. Yun, S. Yoon, K. Kim, Y. R. Do, S.-H. Oh, S.-Y. Jang, *Adv. Energy Mater.* **2016**, *6*, 1502146; b) R. Azmi, S. Y. Nam, S. Sinaga, S.-H. Oh, T. K. Ahn, S. C. Yoon, I. H. Jung, S.-Y. Jang, *Nano Energy* **2017**, *39*, 355 – 362.

[18] J. Burschka, N. Pellet, S.-J. Moon, R. Humphry-Baker, P. Gao, M. K. Nazeeruddin, M. Grätzel, *Nature* **2013**, *499*, 316 – 319.

Manuscript received: August 13, 2017
Revised manuscript received: September 3, 2017
Accepted manuscript online: September 4, 2017
Version of record online: September 21, 2017